FULL PAPER

GaN-on-Si(100)

ADVANCED
FUNCTIONAL
MATERIALS

www.afm-journal.de

Epitaxy of Single-Crystalline GaN Film on CMOS-Compatible Si(100) Substrate Buffered by Graphene

Yuxia Feng, Xuelin Yang,* Zhihong Zhang, Duan Kang, Jie Zhang, Kaihui Liu,* Xinzheng Li, Jianfei Shen, Fang Liu, Tao Wang, Panfeng Ji, Fujun Xu, Ning Tang, Tongjun Yu, Xinqiang Wang, Dapeng Yu, Weikun Ge, and Bo Shen*

Fabricating single-crystalline gallium nitride (GaN)-based devices on a Si(100) substrate, which is compatible with the mainstream complementary metal-oxide-semiconductor circuits, is a prerequisite for next-generation high-performance electronics and optoelectronics. However, the direct epitaxy of single-crystalline GaN on a Si(100) substrate remains challenging due to the asymmetric surface domains of Si(100), which can lead to polycrystalline GaN with a two-domain structure. Here, by utilizing single-crystalline graphene as a buffer layer, the epitaxy of a single-crystalline GaN film on a Si(100) substrate is demonstrated. The in situ treatment of graphene with NH_3 can generate sp^3 C—N bonds, which then triggers the nucleation of nitrides. The one-atom-thick single-crystalline graphene provides an in-plane driving force to align all GaN domains to form a single crystal. The nucleation mechanisms and domain evolutions are further clarified by surface science exploration and first-principle calculations. This work lays the foundation for the integration of GaN-based devices into Si-based integrated circuits and also broadens the choice for the epitaxy of nitrides on unconventional amorphous or flexible substrates.

1. Introduction

GaN-based devices have shown excellent performance in high-frequency and high power devices as well as optoelectronic devices. Si-based electronics offers unsurpassed levels of scaling and functionality. The marriage of GaN-based devices with Si based integrated circuits (ICs) would facilitate a wide range of new chip functionalities that profit from both the excellent optoelectronic/electric applications of GaN and the mature, cost-effective Si complementary metal-oxide-semiconductor (CMOS) technology.[1–4] However, the integration of GaN-based devices into Si ICs remains challenging due to the difficulty in combining these two material systems.

Several approaches have been explored to integrate GaN-based devices with Si substrates. Transfer of GaN layer on to Si via wafer bonding has been realized for many diverse device applications.[5–7] However, the transfer and bonding approaches require complicated process and high cost with limited scalability. In contrast, the direct epitaxy of GaN-based materials on Si is more promising and compatible with the CMOS technology. Epitaxy of GaN on Si(111) has been extensively explored in the past years, and high quality single-crystalline GaN film has been attained.[8,9] However, the monolithic integration of GaN with current CMOS devices requires the growth of single-crystalline GaN on Si(100), the most foundational materials for ICs. Up to now, this approach still remains challenging as considerable hurdles need to be overcome. Si(100) possesses a fourfold symmetry and generates asymmetric surface domains due to surface reconstruction.[10] As schematically exhibited in **Figure 1**b, the Si—Si dimers dangling bonds show a 90° difference from neighboring terraces. GaN/AlN directly grown on Si(100) exhibits 12-fold symmetry with rough surface (see Figure S1a,b, Supporting Information) due to the two-domain structure duplicated from Si(100) surface, as schematically shown in Figure 1a. Although single-domain GaN can be grown on miscut Si(100) substrates, the miscut Si substrates are not compatible with standard CMOS process due to severely anisotropic performance and reliability issues.[11–13] Therefore, it is of great significance to achieve epitaxial single-domain GaN on standard Si(100) substrates in order to integrate GaN-based devices into Si ICs.

A potential way to grow single-domain GaN on standard Si(100) substrate is introducing a buffer layer which can screen the asymmetric surface domains of Si(100) and serve as a template for the epitaxy of GaN. 2D materials are promising candidates owing to the weak van der Waals interactions along the out-of-plane direction. If the interactions between the
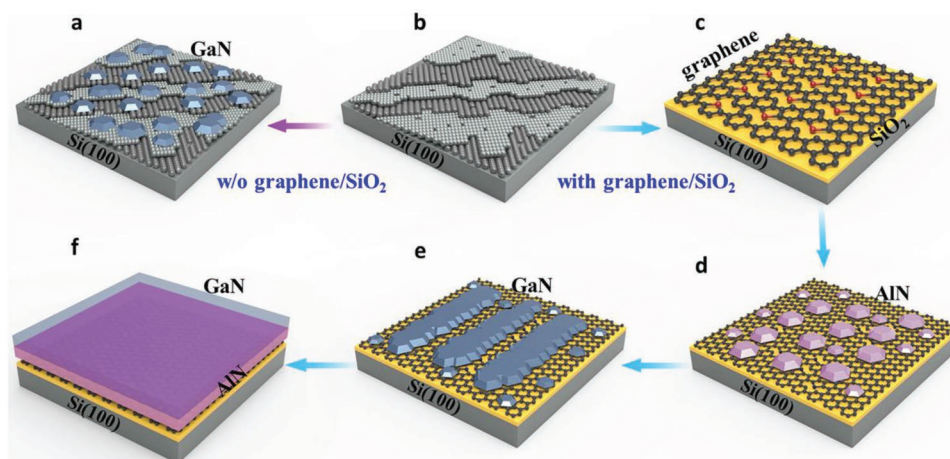
Dr. Y. X. Feng, Dr. X. L. Yang, Dr. Z. H. Zhang, Dr. D. Kang, Dr. J. Zhang, Prof. K. H. Liu, Prof. X. Z. Li, J. F. Shen, F. Liu, Dr. T. Wang, Dr. P. F. Ji, Prof. F. J. Xu, Prof. N. Tang, Prof. T. J. Yu, Prof. X. Q. Wang, Prof. D. P. Yu, Prof. W. K. Ge, Prof. B. Shen
State Key Laboratory of Artificial Microstructure and Mesoscopic Physics
School of Physics
Peking University
Beijing 100871, P. R. China
E-mail: xlyang@pku.edu.cn; khliu@pku.edu.cn; bshen@pku.edu.cn
Prof. X. Q. Wang, Prof. B. Shen
Collaborative Innovation Center of Quantum Matter
Beijing 100871, P. R. China

The ORCID identification number(s) for the author(s) of this article can be found under https://doi.org/10.1002/adfm.201905056.

Figure 1. Schematic diagram of the epitaxy of single-crystalline GaN film on Si(100) without and with single-crystalline-graphene/SiO$_2$ interlayers. a) GaN/AlN directly grown on Si(100). Nitrides nucleate on neighboring terraces with two orientations. b) Surface construction of Si(100). c) Transferred graphene after NH$_3$ pretreatment. d) AlN nucleation islands on graphene. e) GaN strips on the AlN nucleation layer. f) Single-domain GaN film on Si(100) substrate with single-crystalline-graphene/SiO$_2$ interlayers.

substrate and epilayer linked by the 2D buffer layer are well controlled,[14,15] the orientation effect of the Si(100) substrate can be screened. Moreover, the 2D materials with hexagonal crystal structure, such as graphene and hexagonal boron nitride (BN), may guide the growth of wurtzite GaN,[16–19] even the nucleation on graphene is still challenging.

In this work, we achieve the epitaxy of continuous single-crystalline GaN film on Si(100) by using single-crystalline graphene and SiO$_2$ as interlayers. A schematic diagram of the epitaxy process is given in Figure 1. A hybrid buffer consisting of one-atom-thick single-crystalline graphene and a thin SiO$_2$ layer is employed for epitaxy of a single-domain GaN film on Si(100). SiO$_2$ is used to further screen the asymmetric surface domains of the substrate. The single-crystalline monolayer graphene was grown by chemical vapor deposition (CVD) and then transferred to the SiO$_2$/Si(100) surface.[20] We reveal that the nucleation of III-nitrides on graphene is triggered by the formation of sp^3 hybrid C−N bonds on graphene surface. Furthermore, we study the growth mechanism of single-crystalline GaN film on monolayer graphene by investigating the evolution of in-plane orientation with physical characterizations and first-principle calculations. The successful epitaxy of single-crystalline GaN is attributed to the template effect of graphene via the formation of C−N covalent bonds, which serve as driving force for the in-plane alignment of GaN domains. These results verify the orientation effect of 2D graphene on III-nitrides and thus enable the epitaxy of GaN-based devices on Si(100) and other amorphous or flexible substrates.

2. Results and Discussion

2.1. Single-Crystalline GaN Film

The crystal structure and orientation of the epilayers on Si(100) substrate with single-crystalline-graphene/SiO$_2$ interlayers were investigated by X-ray diffraction (XRD). As shown in **Figure 2**a, only the peaks corresponding to wurtzite c-axis GaN can be observed in the 2θ scan. The in-plane orientation of the GaN epilayer was characterized by XRD φ scan on the GaN (103) reflection (Figure 2b). We find six pronounced peaks with intensity maxima at intervals of 60°. This indicates the hexagonal structure and highlights the uniform in-plane alignment of the GaN grown on Si(100) using single-crystalline-graphene/SiO$_2$ interlayers, in contrast to the random in-plane orientated GaN grown on SiO$_2$/Si(100) without the graphene interlayer (see Figure S2, Supporting Information). This implies the excellent orientation effect of the single-crystalline graphene on the nitrides. The single crystallinity of GaN was also confirmed by electron backscatter diffraction maps (see Figure S3, Supporting Information). The scanning electron microscopy (SEM) image reveals the continuity of the GaN film, as shown in Figure 2c. The corresponding atomic force microscopy (AFM) image presents atomic-step terraces, as given in Figure 2d. The root mean square (RMS) roughness of the 2.5 µm thick GaN film is only 0.46 nm in a scanned area of 3 × 3 µm^2. The above results demonstrate that the single-crystalline-graphene/SiO$_2$ are excellent interlayers for the growth of atomically flat single-crystalline GaN film on Si(100) substrate.

Detailed sample structures of the single-crystalline GaN film on Si(100) substrate were analyzed. A low-magnification bright-field scanning transmission electron microscopy (STEM) image shown in Figure 2e gives the sample stack consisting of crystalline Si, amorphous SiO$_2$, and crystalline GaN. The corresponding high-resolution (HR) TEM images of the film and substrate show the clear lattice structure of GaN and Si, respectively. The typical peaks from GaN and sp^2-graphene were simultaneously observed in one Raman spectrum (see Figure S4, Supporting Information), again confirming that GaN was epitaxial grown on the graphene interlayer. Besides the flat surface in the SEM image, the atomic-step terraces in the AFM image, the absence of grain boundaries as well as the low dislocation densities in the STEM image shown in Figure 2e also indicate the high quality of single-crystalline GaN. A wide area cross-sectional HR-TEM image including no dislocations and grain boundaries verified the quality of GaN film too (see Figure S5, Supporting Information).
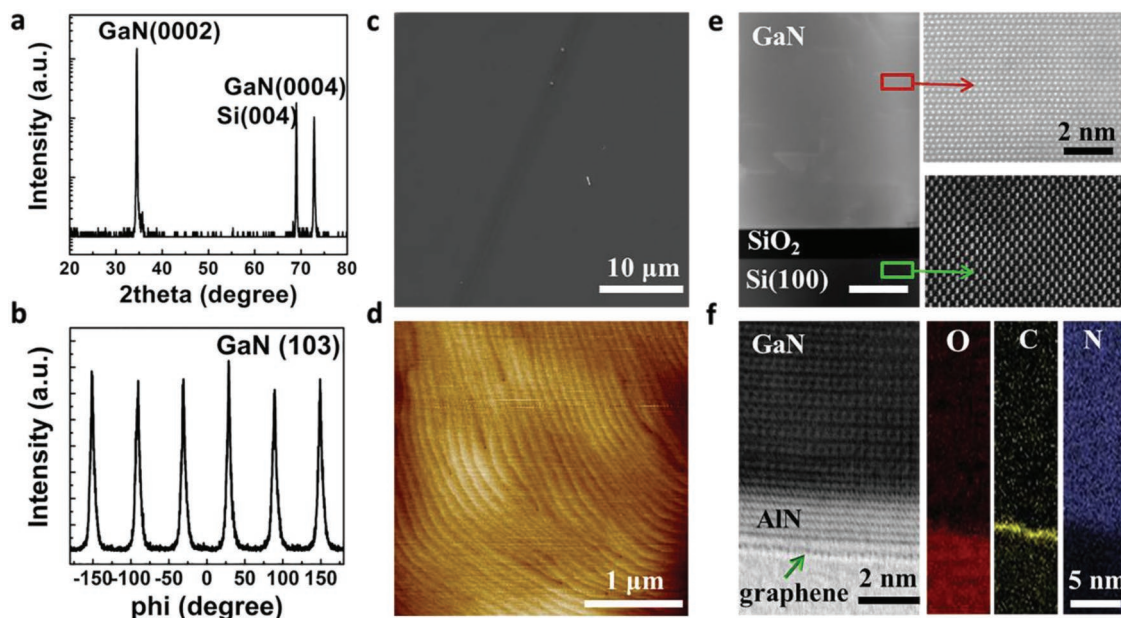
Figure 2. Single crystallinity and sample structure of GaN film on Si(100) with single-crystalline-graphene/SiO$_2$ interlayers. a) XRD omega/2theta scan. Peaks correspond to GaN (0002), Si (004), and GaN (0004), respectively. b) XRD azimuthal off-axis φ scan on GaN (103) reflection shows a sixfold symmetry corresponding to the uniform in-plane alignment. c) Plan-view SEM image of 2.5 μm thick GaN film. d) AFM image of the GaN film, showing a step-flow surface morphology with an RMS of 0.46 nm. e) Cross-sectional STEM image of the sample structure and corresponding HRTEM image showing clear crystal lattice of GaN and Si, respectively. f) Cross-sectional HR-STEM image taken at the interface region, giving the sharp interface structure of the sample. The EELS mapping of the K-edge of O, C, and N at the interface region, confirming the layer structured of graphene.

The interface structure and elemental components of the sample are analyzed by cross-sectional HR-STEM and electron energy loss spectroscopy (EELS) mapping, respectively. The results are shown in Figure 2f. The STEM image clearly shows the atomic planes of the monolayer graphene, AlN, as well as GaN crystal phases. The AlN forms a perfectly sharp and uniform interface to the graphene. The graphene layer still keeps its one-atom-thick nature after the epitaxy process. While EELS is sensitive to light elements with detection limit down to a single-atom layer.[21] To further image the monolayer graphene between the substrate and nitrides, atomic resolution element analysis across the interface region was performed by mapping the O, C, and N elements with EELS. As shown in Figure 2f, a thin carbon layer was clearly mapped using the C K-edge signal, verifying the existence of graphene. Furthermore, the O K-edge signal appears only underneath C (the graphene) while the N K-edge signal appears only above C (the graphene). This suggests that there is no interdiffusion through the graphene during epitaxy. The interface analysis by STEM and EELS indicates that graphene almost remains the layered structure after the epitaxy process, contributing to the sharp interface. Note that the interactions and/or chemical bonds between graphene and nitrides at the interface cannot be detected by STEM and EELS, and thus need further investigation.

2.2. Nucleation and Growth of III-Nitrides on Graphene

We now turn to the nucleation mechanisms of the above nitrides. Since the pristine graphene surface is free of dangling bonds due to its sp^2 bonding configuration, nucleation on graphene is challenging. When nitrides are directly deposited on graphene without any surface treatment, faceted nitrides clusters with rough surface are observed (see Figure S6, Supporting Information). However, by performing the NH$_3$-pretreatment on the pristine graphene, we can observe a remarkably enhanced nucleation of the nitrides. To reveal the nucleation mechanism of nitrides on sp^2-bonded graphene, X-ray photoemission spectroscopy (XPS) studies were carried out to identify the potential bonds between the nitrides and graphene. For the sake of keeping the nitrides/graphene interface within the penetration depth of XPS, AlN with thickness less than 5 nm was deposited both on graphene/Si(100) substrate and Si (111) substrate under the same conditions. As shown in **Figure 3**a, the N 1s of AlN on graphene shows a broad peak in the binding energy (BE) range of 394–402 eV. This peak is deconvoluted by CasaXPS software package into three individual peaks, located at 397.6, 398.7, and 399.6 eV, respectively. The peak at 397.6 eV is also observed for the AlN on conventional Si(111), as shown in Figure 3b, it is thus not related to graphene but could originate from the oxidation of AlN. The other peak in Figure 3b may be attributed to the codeposition of AlN and SiN$_x$ due to the NH$_3$ pretreatment of Si (see Figure S7b, Supporting Information). The peaks at 398.7 and 399.6 eV come from the nitrogen-doped graphene and do not correlate with the underneath layer (see Figure S7a, Supporting Information). The peak at 398.7 eV is assigned to pyridine-like N, corresponding to the sp^2 C−N bonding configuration, while the peak at 399.6 eV indicates the presence of pyrroline-like N corresponding to sp^3 C−N.[22–24] After the NH$_3$ pretreatment of graphene, both sp^2 C−N and sp^3 C−N are formed, as

**ADVANCED
SCIENCE NEWS**
www.advancedsciencenews.com

**ADVANCED
FUNCTIONAL
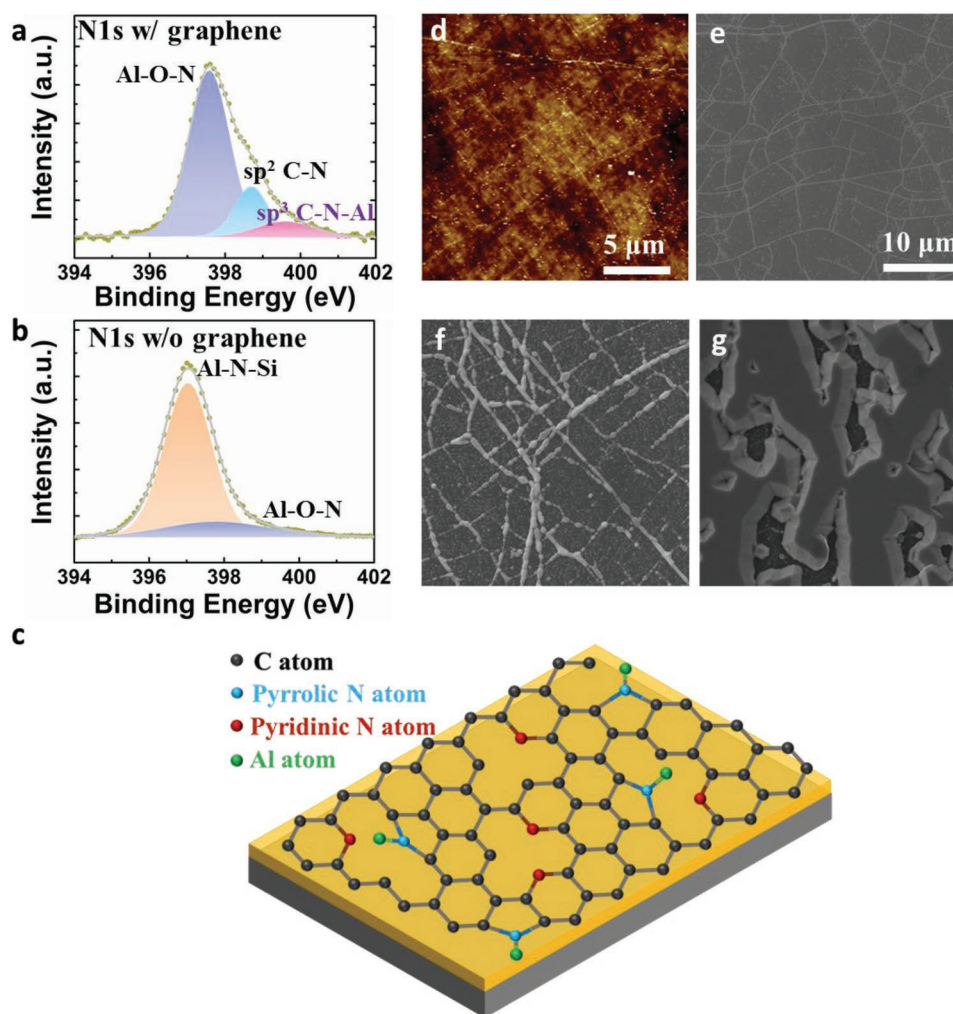MATERIALS**
www.afm-journal.de

Figure 3. Nucleation mechanism and epitaxy process of GaN film on Si(100) with single-crystalline-graphene/SiO$_2$ interlayers. XPS core level spectra with deconvolution of N 1s of a) AlN/graphene/SiO$_2$/Si(100) and b) AlN/Si (111). c) Schematic diagram of the transferred nitrided graphene, the gray, blue, red, and green spheres represent the C, pyrrolic N, pyridinic N, and Al atoms, respectively. d–g) Surface morphology of each growth step, d) AFM image of transferred graphene, e) AlN nucleated on graphene, f) initial growth of GaN on AlN/graphene, and g) a 2.5 µm thick GaN grown with normal V/III.

shown schematically in Figure 3c. Note that the pyrroline-like N in this work locates at a little lower BE than that reported in previous work (399.8–401.2 eV).[24] That is mainly attributed to the growth of AlN on sp^3 C−N because the sp^3 C−N is more reactive than the sp^2 C−N. A three-component system C−N−Al leads to a different bonding environment of N during the epitaxy process. Therefore, we believe that it is the NH$_3$ pretreatment of graphene that generates the sp^3 C−N and hence triggers the nucleation of the nitrides by the formation of C−N−Al.

To gain a deep insight into the epitaxy process of the single-crystalline GaN after the nucleation, growth interruptions at each key process were introduced. The surface morphology of the transferred graphene exhibits high-density of wrinkles (Figure 3d) due to the thermal mismatch between the CVD process and transfer process.[25,26] After depositing AlN, we can find that the nucleation occurs mainly along the wrinkles on the graphene, and there are only a few islands on the flat regions (Figure 3e). Sequentially, at the initial growth stage of GaN (Figure 3f), it also deposits on the AlN mainly along the wrinkles and forms GaN stripes. The GaN stripes show much higher growth rate than the islands on the flat regions of graphene, which should be attributed to the higher AlN nucleation density on the wrinkles. The GaN grown at conventional GaN growth conditions (V/III = 1500) show an uncoalesced surface morphology (Figure 3g) with discrete stripes. This is attributed to the lower density of nuclei on the graphene surface and the lateral growth of GaN is not sufficient to coalesce into a continuous film. In contrast, GaN grown at optimized growth conditions (V/III = 3000) exhibits continuous and smooth surface morphology, as shown in Figure 3g. That could be attributed to the enhanced lateral growth rate at an increased V/III. Therefore, we can conclude that the epitaxy of nitrides on graphene consists of nucleation of AlN on graphene followed by lateral growth of GaN stripes until achieving a continuous and smooth film.

2.3. In-Plane Orientation of III-Nitrides

Having clarified the nucleation mechanisms, we consider the in-plane orientation of the nitrides. First, it should be noted that the monolayer graphene beneath the nitrides cannot be employed for obtaining the in-plane epitaxial relationship between the nitrides and graphene, as the signal from the monolayer graphene is too weak compared to that from the nitrides. But, we suggest that the in-plane epitaxial relationship may be $[1\bar{1}00]_{GaN}//[11\bar{2}0]_{graphene}$ according to previously reports in the case of graphene on SiC and GaN on multilayer graphene.[27,28] As such, we mainly focus on the domain evolutions of the nitrides on the monolayer single-crystalline graphene. It is well recognized that reflection high-energy electron diffraction (RHEED) is a surface sensitive technique and could provide powerful information of the orientation evolution during the growth interruptions. As shown in **Figure 4**a, a clearly spotty

RHEED pattern is observed for AlN on graphene, which remains consistent when rotating the sample at 30° interval. Figure 4b,c gives the RHEED patterns of GaN (Figure 3f) obtained along $[11\bar{2}0]$ and $[1\bar{1}00]$ directions, which keep consistent when rotating the sample at 60° interval. Those are the typical RHEED patterns of single-domain GaN islands. However, the diffraction spots of AlN arise from both $[11\bar{2}0]$ and $[1\bar{1}00]$ directions. That indicates that the AlN consists of two domains with 30° misalignment. It should be declared that the RHEED pattern of AlN comes from all the islands on both the graphene wrinkles and flat regions because of the small thickness of AlN (Figure 3e); while the RHEED patterns of GaN mainly come from the islands on the graphene wrinkles owing to the much higher growth rate than that on the flat graphene (Figure 3f).

Plan-view TEM is further used to characterize the localized in-plane orientation of the GaN domains. Both the wrinkles and flat region where the GaN islands were grown are imaged
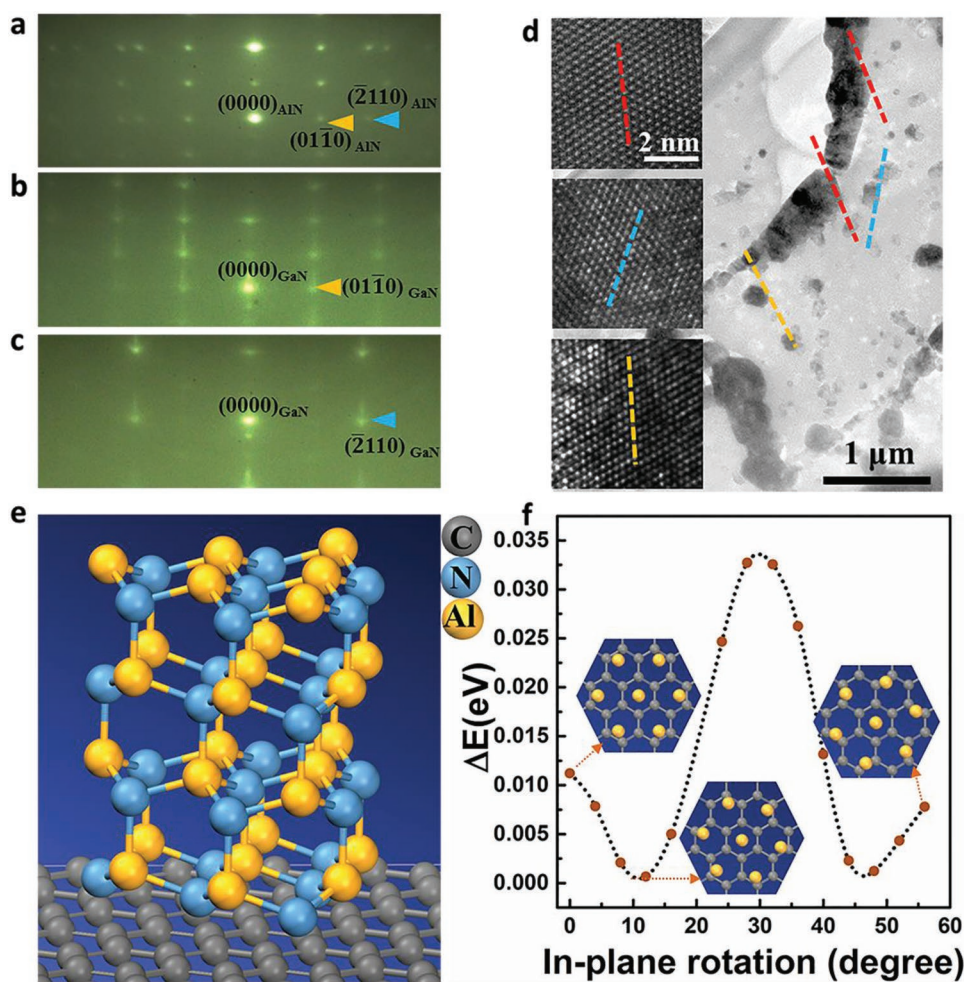

Figure 4. In-plane orientation evolution of single-crystalline GaN film on Si(100) with single-crystalline-graphene/SiO$_2$ interlayers. a) RHEED pattern from AlN nucleated on graphene. The RHEED pattern keeps consistent at 30° interval, which indicates a two-domain structure of AlN. b,c) RHEED patterns of GaN as shown in Figure 3f. The RHEED patterns keep consistent at 60° interval, which indicates the single crystallinity of GaN. The incident direction of the electron beam is b) [11$\bar{2}$0] direction and c) [1$\bar{1}$00] direction. d) Plan-view TEM image of GaN on graphene as shown in Figure 3f. The insets are HRTEM images of GaN islands taken at the red lines, blue line, and yellow line parts, respectively. e,f) DFT calculations of stable configurations of AlN on flat graphene. e) Stable structure of AlN cluster on graphene. C, N, and Al atoms are shown in gray, blue, and yellow, respectively. f) Total energy of different configurations versus in-plane orientation of AlN cluster in the range of 60°. The insets are the corresponding configurations. There are two stable configurations twisted with about 35° rotation.

(Figure 4d). The high-resolution transmission electron microscopy (HRTEM) images shown in the insets were taken from the corresponding part from the plan-view TEM images. As shown in the HRTEM images, the hexagonal arrangement of the atoms corresponds to the *c*-plane of wurtzite GaN. The HRTEM images of the GaN islands on the wrinkles region (as indicated by the red lines in Figure 4d) reveal a completely six-fold in-plane alignment, i.e., a single-domain structure. In contrast, the HRTEM images taken from the GaN islands on the flat regions (as indicated by blue and yellow lines in Figure 4d) indicate a two-domain structure with 30° rotation. Since the orientation of GaN follows the crystalline properties of AlN, the above results indicate that the AlN nucleated on the graphene wrinkles exhibit a single-domain structure while those on the flat regions show a two-domain structure.

As the graphene serves as the actual epitaxial substrate, the orientation effect of graphene on nitrides should be established. The crystallographic direction of an epilayer depends not only on the crystal orientation of the substrate but also on the atomic interactions between the substrate and epilayer. The graphene wrinkles can be ascribed to defective C−C bonds, which are asymmetric and ready to be substituted by N atoms.[29,30] Considering the sp³ C−N revealed by XPS, it is reasonable to believe that N atoms prefer to substitute the C atoms on the wrinkles and form sp³ C−N, which triggers the high nucleation density of AlN over there. When the nitrides nucleate on flat graphene, it is difficult to form chemical bonds due to the lack of sp³ C−N. The structure and stability of AlN on flat graphene were studied using density functional theory (DFT) calculations. First, we have performed the total energy calculations of the structures with different adsorbed atoms on graphene, i.e., Al and N atoms, respectively. The calculation results show that, for wurtzite AlN on graphene, the adsorption of N atoms on graphene shows a better stability than the Al atoms on graphene, as schematically illustrated in Figure 4e. Second, a series of calculations with different adsorption distances, i.e., 2.0, 3.0, 3.5, and 4.0 Å, between AlN and graphene have been conducted. It is proved that 3.0 Å is about the optimal distance between AlN and graphene. Additionally, the total energies of different configurations with various in-plane orientations in the range of 0°–60° were calculated by taking the Van der Waals interactions into account. The results are shown in Figure 4f. In the 0° configuration, one Al atom lies in the hollow site of graphene, and the other six Al atoms align on the bridge sites. Within the range of 60° in-plane rotations, there exist two different configurations with almost the same minimized total energy. The in-plane rotations angle between these two stable configurations is calculated to be about 35°, which is consistent with those experimentally observed on flat graphene. On the other hand, the nitrides easily nucleate on graphene wrinkles, where the covalent bonds form between AlN and graphene because of the sp³ C−N. Because the directional character of the covalent bonds has strong orientation effect on the epilayer,[31] the nitrides maintain the same crystalline properties with graphene in this case. That is the exact reason why the GaN and AlN on the single-crystalline graphene wrinkles exhibit single-domain structure and finally coalesced to single-crystalline GaN film, while the GaN on polycrystalline graphene which consists of two domains with 30° misalignment shows polycrystalline characteristics with two-domain structure (see Figure S8, Supporting Information).

3. Conclusion

In summary, we achieve the epitaxy of single-crystalline GaN film with step-flow surface on CMOS-compatible Si(100) substrates by using single-crystalline-graphene/SiO₂ buffer layer. We revel that the in situ treatment of graphene with NH₃ can generates sp³ C−N bonds, which then triggers the nucleation of the nitrides. Owing to the high nucleation density of AlN with single-domain structure on the graphene wrinkles, which reserves the orientation property of the single-crystalline graphene, the subsequent GaN islands possess a higher growth rate and can thus coalesce to a continuous single-crystalline GaN film. This work not only paves the way for the integration of GaN-based devices into Si-based ICs but also highlights the prospects for the epitaxy of wafer-scale single-crystalline GaN film on amorphous substrates.

4. Experimental Section

Graphene Preparation and Epitaxy of GaN: High quality single crystallinity graphene was grown on single-crystal Cu (111) substrate by CVD. The graphene was then transferred onto Si(100) substrate which is covered by about 100 nm thick amorphous SiO₂ layer. More details can be found in our previous work.[20] After the transfer, the substrate was loaded into metal organic chemical vapor deposition (Aixtron close coupled showerhead (CCS) 3 × 2 in. system). Trimethylgallium, trimethylaluminum, and ammonia were used as precursors for gallium, aluminum, and nitrogen, respectively. Hydrogen was used as the carrier gas. Before epitaxy of the nitrides, a step of nitridation was performed with an NH₃ flow of 800 sccm for 10 min at high temperature (>1100 °C). Subsequently, an AlN nucleation layer (≈10 nm thick) was grown at V/III of ≈450 followed by GaN layer (≈2.5 μm) grown at a high V/III of ≈3000 to promote the lateral growth.

Plan-View TEM Sample Preparation: For the preparation of the plan-view TEM sample, a copper grid was first fixed onto the GaN side (Figure 3f). Then the whole stack including Si(100)/SiO₂/graphene/AlN/GaN/Cu grid was dipped into dilute HF solution to etch the SiO₂ layer. Finally, the Cu grid/GaN/AlN/graphene was released from the Si(100) substrate.

Computational Model: The DFT calculations were performed with the Vienna ab initio simulation package,[32] using projector augmented wave pseudopotentials.[33] The Perdew—Burke—Ernzerhof exchange correlation functional was employed,[34] expanding the wave functions in the plane wave basis up to a cutoff energy of 800 eV. The Van der Waals corrections are included to count for the interlayer interactions.[35] In the calculations, the separately optimized structure of AlN and graphene together as the initial configurations was put. Owing to a large number degrees of freedom and accompanied large computational cost, constrains of the exploration of the energy landscape to the adsorbed atoms, adsorption distance, and in-plane rotation angle between AlN and graphene were put. In the optimizations of graphene and AlN, the thresholds for the electronic energy and forces were set to be 5×10^{-6} eV and 0.01 eV Å⁻¹, respectively. The optimized parameters of bulk AlN are $a = b = 3.128$ Å, $c = 5.017$ Å, the distance between Al and N atoms along out-of-plane direction is 1.914 Å, along with $9 \times 9 \times 6$ Monkhorst-Pack mesh sampling in the reciprocal space. The optimized lattice parameters of graphene are $a = b = 2.467$ Å, and the C−C bond length is 1.424 Å. A simulation box consisting of 364-atoms graphene and 26-atoms Al and 26-atoms N, with fixed edge lengths of $a = 32.065$ Å, $b = 29.905$ Å, and $c = 37.000$ Å was employed. The vacuum above the top of AlN is about 20 Å. The k-space integration of the simulation box was done with a single Γ point.

Supporting Information

Supporting Information is available from the Wiley Online Library or from the author.

Acknowledgements

Conflict of Interest

The authors declare no conflict of interest.

Keywords

in-plane orientation, nucleation, Si(100), single-crystalline GaN films, single-crystalline graphene

[1] T. Li, M. Mastro, A. Dadgar, *III–V Compound Semiconductors: Integration with Silicon-Based Microelectronics*, CRC Press, Parkway, NW **2012**.

[2] Y. Sun, K. Zhou, Q. Sun, J. Liu, M. Feng, Z. Li, Y. Zhou, L. Zhang, D. Li, S. Zhang, M. Ikeda, S. Liu, H. Yang, *Nat. Photonics* **2016**, *10*, 595.

[3] H. Amano, Y. Baines, E. Beam, M. Borga, T. Bouchet, P. R. Chalker, M. Charles, K. J. Chen, N. Chowdhury, R. Chu, C. D. Santi, M. M. D. Souza, S. Decoutere, L. D. Cioccio, B. Eckardt, T. Egawa, P. Fay, J. J. Freedsman, L. Guido, O. Häberlen, G. Haynes, T. Heckel, D. Hemakumara, P. Houston, J. Hu, M. Hua, Q. Huang, A. Huang, S. Jiang, H. Kawai, D. Kinzer, M. Kuball, A. Kumar, K. B. Lee, X. Li, D. Marcon, M. März, R. McCarthy, G. Meneghesso, M. Meneghini, E. Morvan, A. Nakajima, E. M. S. Narayanan, S. Oliver, T. Palacios, D. Piedra, M. Plissonnier, R. Reddy, M. Sun, L. Thayne, A. Torres, N. Trivellin, V. Unni, M. J. Uren, M. V. Hove, D. J. Wallis, J. Wang, J. Xie, S. Yagi, S. Yang, C. Youtsey, R. Yu, E. Zanoni, S. Zeltner, *J. Phys. D: Appl. Phys.* **2018**, *51*, 163001.

[4] B. Leung, J. Song, Y. Zhang, J. Hang, *Adv. Mater.* **2013**, *25*, 1285.

[5] K. H. Lee, S. Bao, L. Zhang, D. Kohen, E. Fitzgerald, C. S. Tan, *Appl. Phys. Express* **2016**, *9*, 086501.

[6] J. W. Chung, J. K. Lee, E. L. Piner, T. Palacios, *IEEE Electron Device Lett.* **2009**, *30*, 1015.

[7] C. Xiong, W. Pernice, K. K. Ryu, C. Schuck, K. Y. Fong, T. Palacios, H. X. Tang, *Opt. Express* **2011**, *19*, 10462.

[8] D. Zhu, D. J. Wallis, C. J. Hunphreys, *Rep. Prog. Phys.* **2013**, *76*, 106501.

[9] J. Cheng, X. Yang, L. Sang, L. Guo, A. Hu, F. Xu, N. Tang, X. Wang, B. Shen, *Appl. Phys. Lett.* **2015**, *106*, 142106.

[10] D. E. Aspnes, J. Ihm, *Phys. Rev. Lett.* **1986**, *57*, 3054.

[11] V. Lebedev, J. Jinschek, J. Kräußlich, U. Kaiser, B. Schröter, W. Richter, *J. Cryst. Growth* **2001**, *230*, 426.

[12] J. E. Chung, J. Chen, P. K. Ko, C. Hu, M. Levi, *IEEE Trans. Electron Devices* **1991**, *38*, 627.

[13] G. Qin, H. Zhou, E. B. Ramayya, Z. Ma, I. Knezevic, *Appl. Phys. Lett.* **2009**, *94*, 073504.

[14] Y. Kim, S. S. Cruz, K. Lee, B. O. Alawode, C. Choi, Y. Song, J. M. Johnson, C. Heidelberger, W. Kong, S. Choi, K. Qiao, I. Almansouri, E. A. Fitzgerald, J. Kong, A. M. Kolpak, J. Hwang, J. Kim, *Nature* **2017**, *544*, 340.

[15] W. Kong, H. Li, K. Qiao, Y. Kim, K. Lee, Y. Nie, D. Lee, T. Osadchy, R. J. Molnar, D. K. Gaskill, R. L. M. Ward, K. M. Daniels, Y. Zhang, S. Sundram, Y. Yu, S. H. Bae, S. Rajan, Y. S. Horn, K. Cho, A. Ougazzaden, J. C. Grossman, J. Kim, *Nat. Mater.* **2018**, *17*, 999.

[16] J. Kim, C. Bayram, H. Park, C. W. Cheng, C. Dimitrakopoulos, J. A. Ott, K. B. Reuter, S. W. Bedell, D. K. Sadana, *Nat. Commun.* **2014**, *5*, 4836.

[17] M. Heilmann, A. M. Munshi, G. Sarau, M. Göbelt, C. Tessarek, V. T. Fauske, A. T. J. Helvoort, J. Yang, M. Latzel, B. Hoffmann, G. Conibeer, H. Weman, S. Christiansen, *Nano Lett.* **2016**, *16*, 3524.

[18] Y. Xu, B. Cao, Z. Li, D. Cai, Y. Zhang, G. Ren, J. Wang, L. Shi, C. Wang, K. Xu, *ACS Appl. Mater. Interfaces* **2017**, *9*, 44001.

[19] K. Chung, H. Oh, J. Jo, K. Lee, M. Kim, G. C. Yi, *NPG Asia Mater.* **2017**, *9*, e410.

[20] X. Xu, Z. Zhang, J. Dong, D. Yi, J. Niu, M. Wu, L. Lin, R. Yin, M. Li, J. Zhou, S. Wang, J. Sun, X. Duan, P. Gao, Y. Jiang, X. Wu, H. Peng, R. S. Ruoff, Z. Liu, D. Yu, E. Wang, F. Ding, K. Liu, *Sci. Bull.* **2017**, *62*, 1074.

[21] K. Suenaga, M. Tencé, C. Mory, C. Colliex, H. Kato, T. Okazaki, H. Shinohara, K. Hirahara, S. Bandow, S. Iijima, *Science* **2000**, *290*, 2280.

[22] D. Wei, Y. Liu, Y. Wang, H. Zhang, L. Huang, G. Yu, *Nano Lett.* **2009**, *9*, 1752.

[23] G. Sarau, M. Heilmann, M. Bashouti, M. Latzel, C. Tessarek, S. Chistiansen, *ACS Appl. Mater. Interfaces* **2017**, *9*, 10003.

[24] H. Wang, T. Maiyalagan, X. Wang, *ACS Catal.* **2012**, *2*, 781.

[25] S. Deng, V. Berry, *Mater. Today* **2016**, *19*, 197.

[26] V. E. Calado, G. F. Schneider, A. M. M. G. Theulings, C. Dekker, L. M. K. Vandersypen, *Appl. Phys. Lett.* **2012**, *101*, 103116.

[27] A. Ouerghi, M. G. Silly, M. Marangolo, C. Mathieu, M. Eddrief, M. Picher, F. Sirotti, S. E. Moussaoui, R. Belkhou, *ACS Nano* **2012**, *6*, 6075.

[28] H. Hayashi, Y. Konno, K. Kishino, *Nanotechnology* **2016**, *27*, 055302.

[29] F. Banhart, J. Kotakoski, A. V. Krasheninnikov, *ACS Nano* **2011**, *5*, 26.

[30] K. Kim, H. B. R. Lee, R. W. Johnson, J. T. Tanskanen, N. Liu, M. G. Kim, C. Pang, C. Ahn, S. F. Bent, Z. Bao, *Nat. Commun.* **2014**, *5*, 4781.

[31] I. Markov, S. Stoyanov, *Contemp. Phys.* **1987**, *28*, 267.

[32] G. Kresse, J. Hafner, *Phys. Rev. B* **1994**, *49*, 14251.

[33] P. E. Blöchl, *Phys. Rev. B* **1994**, *50*, 17953.

[34] J. P. Perdew, K. Burke, M. Ernzerhof, *Phys. Rev. Lett.* **1997**, *7*, 3865.

[35] S. Grimme, *J. Comput. Chem.* **2006**, *27*, 1787.